Available online at www.sciencedirect.com
ScienceDirect
Ceramics International 36 (2010) 733–740
CERAMICS INTERNATIONAL
www.elsevier.com/locate/ceramint

Microstructural characterization of alkali metal mediated high temperature reactions in mullite based refractories

J. Stjernberg [a,*], B. Lindblom [b], J. Wikström [b], M.-L. Antti [a], M. Odén [c]

[a] Division of Engineering Materials, Luleå University of Technology, 971 87 Luleå, Sweden
[b] LKAB, 971 28 Luleå, Sweden
[c] Nanostructured Materials, Dept. of Physics, Linköping University, 581 83 Linköping, Sweden

Received 27 August 2009; received in revised form 9 September 2009; accepted 4 October 2009
Available online 3 November 2009

Abstract

Two types of refractory bricks were used in reaction tests with slag from a production kiln for iron ore pellet production. Electron microscopy was used to characterize morphological changes at the slag/brick interface and active chemical reactions. Phases such as kalsilite, nepheline and potassium β-alumina form, in a layered structure, as a consequence of alkali metals migration in the brick. Larger hematite grains (50–100 μm) in the slag remain at the original slag/brick interface, while smaller grains dissolve and move through the partly dissolved brick bulk, and forms micrometer sized needle-shaped crystals deeper in the lining material. Thermodynamic simulations predict the formation of a solid solution between hematite and corundum which is also observed in the reaction zone after extended time periods.

Keywords: B. Electron microscopy; D. Mullite; D. Al_2O_3; E. Refractories

1. Introduction

Refractories based on ceramic materials have been used in metallurgical processes since around 3500 BC when metals were first extracted from ores. Today there is an ongoing development of new refractories, but traditional alumina silicate refractories are still in widespread use, especially in the iron- and steelmaking industry, which uses 70% of all refractories [1].

The pelletizing of iron ore as a burden material for blast furnaces was first patented 1912 by A.G. Andersson and the first commercial plant started in Minnesota, 1952. Two main processes used during such production today are: the traveling grate, and the grate–kiln process [2], where the grate is a roaster furnace and the kiln is a rotating furnace insulated with refractory bricks. Temperatures up to about 1350 °C can be reached in the kiln [3]. The first iron ore pellet plant of grate–kiln type started in 1960 and today there are globally 35 such Allis-Chalmers type pellet plants and a few of other types.

Refractory bricks wear need to be replaced after some time when exposed to a corrosive atmosphere at high temperatures. In rotary kilns the wear situation is complex since several different mechanisms operates simultaneously. The main source for corrosion and wear is residues from the pellet production that together with fly ash from coal burned to heat the kiln forms a so-called slag that accumulates in chunks on the bricks. This phenomenon with adhesion of deposits on the refractories is observed at different iron ore production sites and types of kilns, and it seems to be related to the quality and composition of the burner fuel [4].

Two common brick types used in such kilns have been used in this lab scale study. The dominant constituents in both brick types are alumina (Al_2O_3) and silica (SiO_2) in different amounts, but there are also traces of other oxides present. Al_2O_3 and SiO_2 in the ratio 3/2 forms the mineral mullite during heat treatment, which has appropriate refractory properties, among them high melting temperature, low thermal expansion and low thermal conductivity. Mullite is a solid solution where the amount of Al_2O_3 can vary between 55 and 90 wt%, but it is commonly expressed stoichiometrically by the oxide formula $3Al_2O_3{\cdot}2SiO_2$ [5].

In general, the most harmful wear mechanism of refractory bricks in this application, is a combination of mechanical

* Corresponding author. Tel.: +46 920 492 358; fax: +46 920 491 084.
E-mail address: jesper.stjernberg@ltu.se (J. Stjernberg).

0272-8842/$36.00
doi:10.1016/j.ceramint.2009.10.018

strength degradation caused by the slag and thermal shock [6]. The brick degradation is caused by concurrently active processes of chemical reactions and migration of grains from the refractory lining into flow of viscous molten slag [7].

During a chemical attack caused by alkali metal containing slag, mullite refractories corrode and some specific phase transformations occur. When alkali metal reacts with aluminosilikates, the feldspathoids nepheline ($NaAlSiO_4$), kalsilite ($KAlSiO_4$) and leucite ($KAlSi_2O_6$) are commonly formed [8], while the formation of the alkali feldspars orthoclase ($KAlSi_3O_8$) and albite ($NaAlSi_3O_8$) depend on time and the presence of free SiO_2, and jadeite ($NaAlSi_2O_6$) forms only under high pressure [9]. The formation of these phases is assumed to contribute to the degradation of the bricks. However, proper descriptions of the wear mechanisms are still lacking to facilitate improved lifetime through proper brick design. Thus, this paper gives detailed descriptions of the chemical reactions occurring at the interface between the brick and alkali metal containing slags. The reaction zone is characterized after different types of heat treatments by X-ray diffraction (XRD) and electron microscopy and spectroscopy (QEMSCAN and SEM), and the experimentally observed reaction products are compared to thermodynamic simulations of the same system.

2. Experimental procedure

Two different types of bricks were used in this study, one based on bauxite (product name: Victor HWM, Höganäs Bjuf) and on andalusite (product name: Silox 60, Höganäs Bjuf). The chemical compositions of the bricks, based on datasheets from the producer, are shown in Table 1. Their porosity is between 15% and 20% and their density is 2500–3000 kg/m^3. The slag used in this study was collected at the outlet of a production kiln located in Svappavaara (LKAB), Sweden, during a production stop. Additives used were K_2CO_3 and Na_2CO_3 (both from Merck, 99.9 wt% purity).

The reactions between brick material and slag were conducted through a series of crucible/slag reaction tests. Crucibles were machined from both brick types in their as fabricated condition, with dimensions of 40 mm × 40 mm × 50 mm. The diameter of the cavity was 16 mm, with a depth of 25 mm. Each cavity was filled with a milled 8 g powder mixture comprised of slag, 5 wt% sodium and 5 wt% potassium, both in the form of carbonates. The crucibles were heated to different temperatures near the process temperature in the kiln for different holding times. After heat treatment, the crucibles were cut into two parts along the center of the cavity, to facilitate investigation of the slag/brick interface. The interfaces were polished and carbon sputter deposited prior to electron microscopy.

Table 1
Chemical composition of refractory bricks used in this study.

wt%	Victor HWM	Silox 60
Al_2O_3	~73	~60
SiO_2	~26	~37
CaO	0.2	0.1
TiO_2	2.7	1.5
Fe_2O_3	1.1	0.9
Alkalis	0.3	0.5

The chemical composition of the slag was determined by X-ray fluorescence spectroscopy (XRF) using rhodium X-ray radiation, a flow proportional counters for Na, Mg and Al and a scintillation counter for all other elements over a 2θ-interval of 22–145°, using a PANalytical MagiX instrument.

The X-ray diffraction experiments were conducted on as fabricated bricks, milled to a powder, with a Philips X-ray diffractometer (MRD) instrument, using Cu Kα radiation. The diffractograms were recorded over an interval 10–90° of 2θ. Scanning electron microscopy (SEM) studies were carried out in a JEOL JSM-6460 (software INCA), equipped with energy dispersive spectroscopy (EDS). To map the location and chemical composition of the minerals present in the sample, quantitative mineralogical evaluations using a QEMSCAN® system were performed. The system is based upon a Zeiss E340 scanning electron microscope with four energy dispersive X-ray spectrometers (EDS). The resulting X-ray and back-scattered electron (BSE) signals are compared with a database of known minerals and amorphous phases to produce a mineralogical identification [10–12]. Species with similar EDS-spectrum such as magnetite and hematite, can be differentiated by different BSE signal, while it is still difficult to separate magnetite and wüstite, since the software does not differentiate crystal structures [13]. Several studies have been performed using this type of instrument, for different mineralogical systems, such as aluminosilicates in fly ash [14], kimberlite ores [15], and gold-bearing ores [16]. In this study phase maps were recorded based upon point analysis with a step size of 7 μm.

A mineral database – Species Identification Protocol (SIP) – was used in the QEMSCAN® studies for phase identification. The SIP is built by the user to describe the different minerals and slags. These include amorphous phases, boundary phases and minerals with impurities. In this work special attention was given to the definitions of complex slag phases, hematite, corundum and mullite, all with variable composition. The SIP was built using detailed X-ray spectra which were collected at different sample areas of interest. For phase identification, the software works through the SIP from top to bottom and defines the measurement according to first match. The SIP is sorted with the minerals first, followed by defined slags and other undefined groups. Table 2 gives the compositions of the modified SIP-entries used in this study.

Thermodynamic simulations were carried out with the software Factsage, version 5.5 (Thermfact/CRCT, GTT-Technologies) using the equilibrium package. A complex system such as a refractory-slag system never reaches equilibrium, but simulations were performed to give an indication of which phases that represent the end points of the reactions. The simulations were performed in the temperature range between 500 and 1400 °C, in inert atmosphere at ambient pressure.

Table 2
Composition in wt% for modified entries in the species identification protocol (SIP) used in the QEMSCAN analysis.

	Al_2O_3	SiO_2	Fe_2O_3	K_2O	Na_2O
Alumina silicate matrix	25 ± 5	40 ± 5	10 ± 3.5	15 ± 6	10 ± 3.5
Slag (Al–Fe)	30 ± 5	25 ± 5	25 ± 3.5	10 ± 6	10 ± 3.5
Slag (Al–Si)	45 ± 5	30 ± 5	10 ± 3.5	10 ± 3	5 ± 3.5
Hematite (Al)	35 ± 5		50 ± 7	10 ± 3	
Hematite (Al–K)	45 ± 5		50 ± 3.5	10 ± 3	
Mullite needles in alkali glass	50 ± 5	30 ± 5	5 ± 3.5	10 ± 3	5 ± 3.5
Mullite	60 ± 5	40 ± 5			
Mullite (Ca–K)	65 ± 5	5 ± 5	7 ± 7	20 ± 6	5 ± 3.5
Corundum	100 ± 5				
Corundum (K)	70 ± 10	5 ± 5	10 ± 10	10 ± 3	5 ± 3.5
Corundum (Fe)	85 ± 5		15 ± 3.5		
Corundum (high Fe)	55 ± 5		40 ± 7	10 ± 3	

Table 3
Chemical composition of the slag used in the experiments.

Fe_2O_3	SiO_2	Al_2O_3	MgO	CaO	FeO	TiO_2	Na_2O	K_2O	V_2O_5	MnO	P_2O_5
92.45	3.11	0.99	1.38	0.58	0.54	0.29	0.128	0.102	0.19	0.09	0.053

3. Results

The composition of the slag used in the tests is presented in Table 3. The slag is assumed to be fully oxidized, thus its composition is presented as oxides (in wt%).

The X-ray diffractograms of powders of milled bricks Victor HWM and Silox 60 in their as received condition show that mullite and corundum are present in both brick types (Fig. 1). In addition both bricks contain traces of other oxides, including quartz.

Fig. 2 depicts graphically the mineral assays detected by QEMSCAN of the investigated samples and the minerals concentrations. The color codes used in Fig. 2 are also used in the field images (Figs. 3 and 4). Abbreviations used in the figure are—V: bauxite based brick and S: andalusite based brick, e.g. S(24)1400 should be read as crucible made from the andalusite based brick tested at 1400 °C for 24 h.

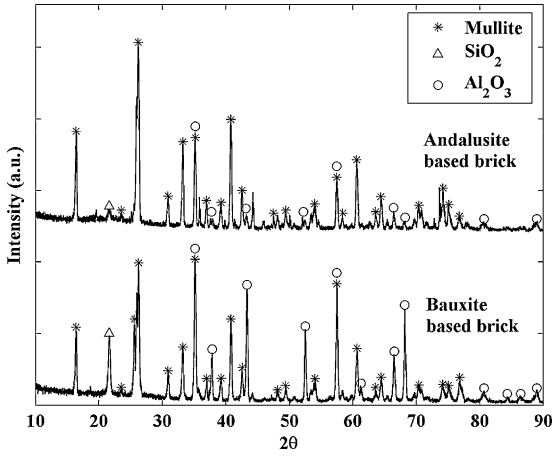

Fig. 1. XRD diffractogram of the original brick materials Victor HWM and Silox 60.

The mineral assays are generated from a frame size of a minimum of 0.5 cm^2. The mineral assays confirm that both brick types in their as received condition contain primarily corundum and mullite (corundum, mullite and mullite (Ca–K)). The bauxite based brick has a higher Al_2O_3 content which is seen in Fig. 2 as a higher corundum content. In the case of the reactions zones, the mineral assays should be read with some caution since the volume fractions of the formed phases are strongly related to the frame size. However, for the brick based on bauxite the major reaction products are: corundum (K), corundum (Fe), alumina silicate matrix, mullite needles in alkali glass and slag (Al–Fe), and for the andalusite based brick: alumina silicate matrix, slag (Al–Fe) and slag (Al–Si). Also some hematite from the added slag is found in the samples such as hematite and hematite (Al).

3.1. Brick–slag interface characterization

Fig. 3 shows QEMSCAN micrographs of the interaction zones between bauxite based brick and slag, after 5 (Fig. 3(a)) and 72 h (Fig. 3(b)) at 1400 °C. After 5 h hematite is dominating at the surface. Below the surface several layers have evolved, first two layers mainly consisting of hematite (Al) and hematite (Al–K). Below the hematite zone corundum (high Fe) and slag (Al–Fe) are present and even deeper layers of corundum (K) and slag (Al–K) are observed. A reaction layer has formed between the hematite and corundum zones. Deeper into the brick alkali metal has penetrated further and is found mainly as mullite needles in alkali glass. The corundum grains are intact and some alkali metal has migrated along the grain boundaries. In addition, closely related to the alkali metal

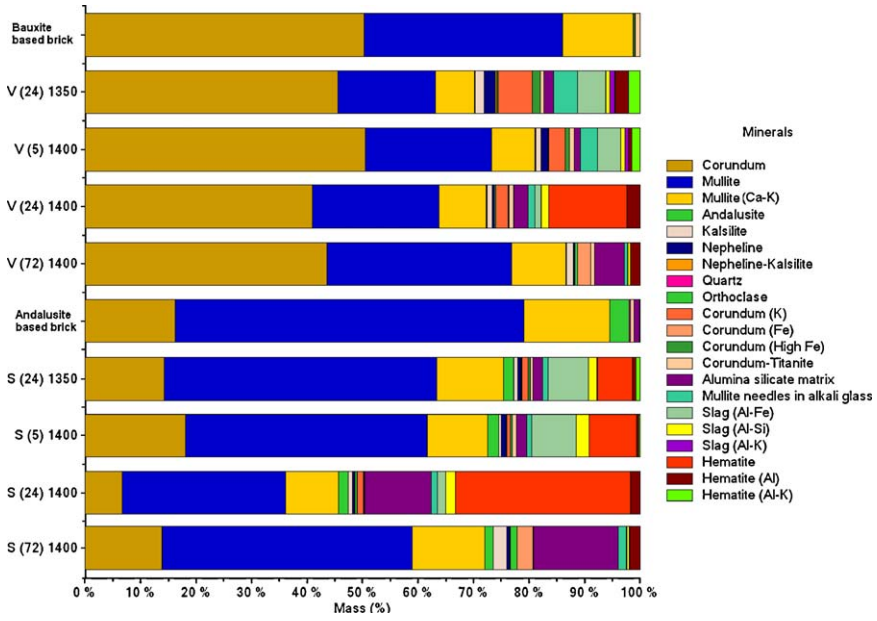

Fig. 2. Mineral assay of different minerals and phases from the QEMSCAN analysis.

migration fronts the phase potassium β-alumina and the feldspathoid minerals kalsilite and nepheline are formed.

After heat exposure for 72 h (Fig. 3(b)) hematite is dominating together with needles of corundum (Fe) at the surface. Further down, a corundum and mullite zone is present. Below a zone with corundum and alumina silicate matrix is present. The corundum and hematite solid solution, corundum (Fe), has increased in concentration compared to 5 h test, seen as needle-like formations at the surface. The reaction layer is more diffused here. Much of the alkali metal is present in the alumina silicate matrix which is distributed over a relatively large area.

QEMSCAN micrographs in Fig. 4 shows the interaction zones between the andalusite based brick and slag, after 5 (a) and 72 h (b) at 1400 °C. At the surface in the 5 h test, hematite is dominating together with the slag (Al–Fe). Further into the reaction zone the slag (Al–Fe) is still present together with hematite (Al–K) and corundum (high Fe). Closer to the mullite area a zone of corundum (K) and slag (Al–Si) is found. A distinct reaction layer has formed between the hematite and corundum/mullite. Below this reaction layer a crack is seen between the layer and the bulk of the brick material. Alkali metal penetration further into the bulk material is less

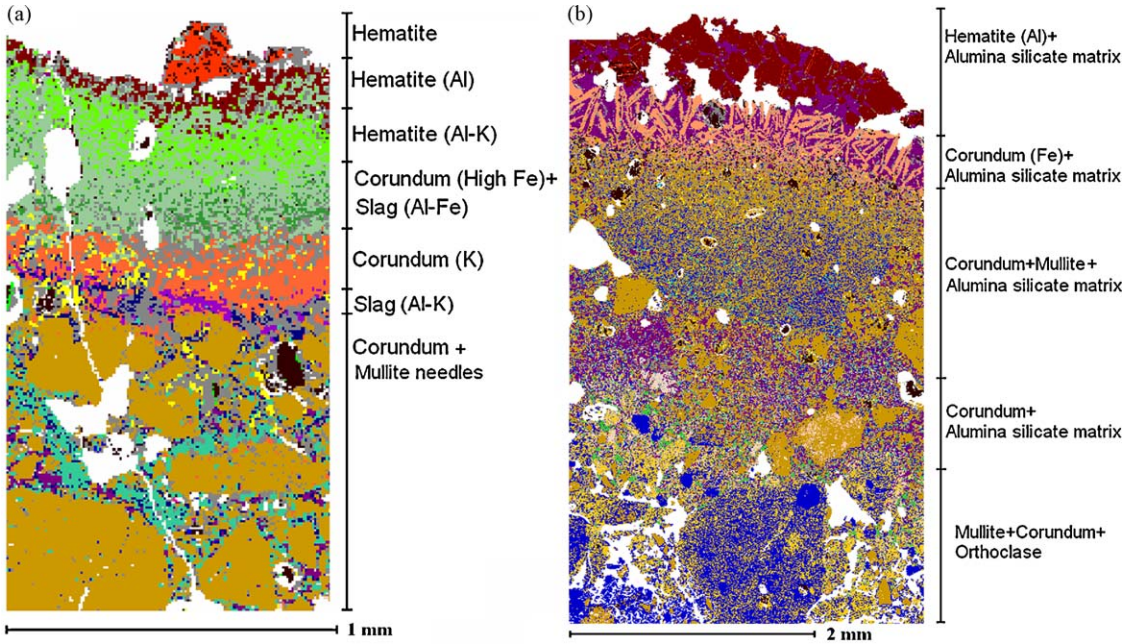

Fig. 3. Phase maps generated by QEMSCAN field image scans showing Victor HWM and the interaction zone with the slag after 5 (to left) and 72 (to right) hours at 1400 °C. Identified phases in different reaction zones are given to the right of the images.

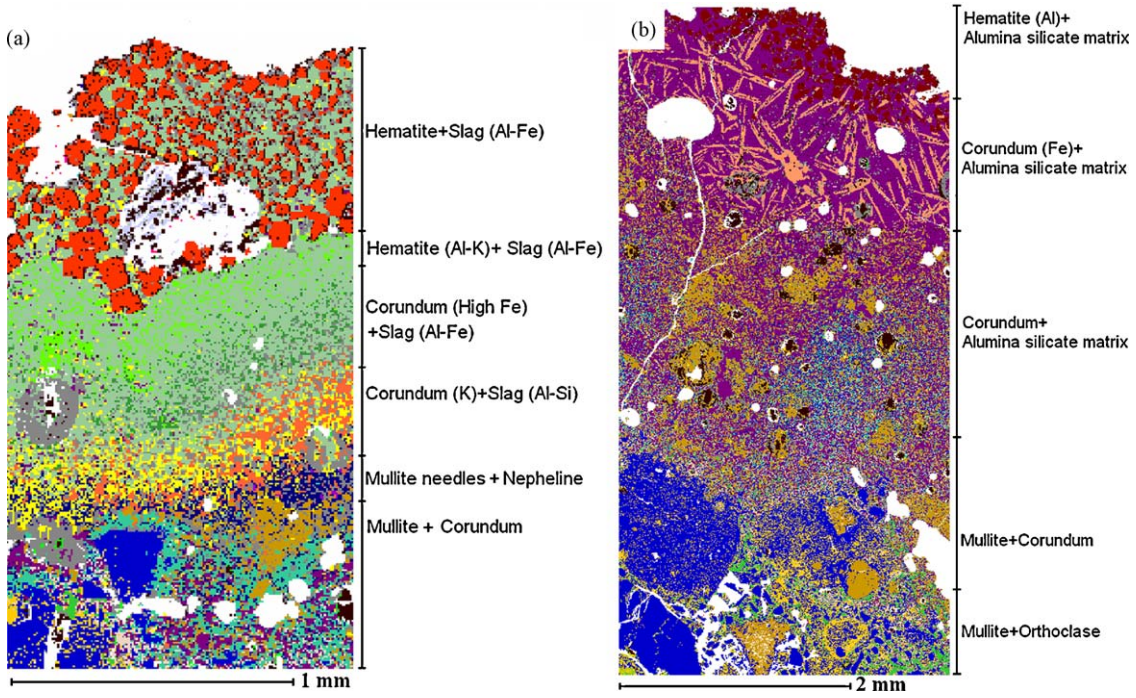

Fig. 4. Phase maps generated by a QEMSCAN field image scans showing Silox 60 and the interaction zone with the slag 5 (to left) and 72 (to right) hours at 1400 °C. Identified phases in different reaction zones are given to the right of the images.

pronounced with increasing depth, and mullite and corundum grains are intact.

At the surface in the 72 h test, hematite (Al) is dominating at the surface together with needles of corundum (Fe), below which a zone with corundum and alumina silicate matrix is present. A third and fourth layer are dominated by corundum and mullite, and corundum and orthoclase, respectively. The surface contains adhered hematite with corundum and hematite solid solution needles. The reaction layer is more diffused in this test, compared to samples with 5 h dwell time. A majority of the alkali metal is present in the alumina silicate matrix which is distributed across the entire reaction zone.

High resolution analysis performed by SEM/EDS shows the migration of hematite through the partly dissolved and porous brick bulk by capillary infiltration and diffusion. It appears as needle-shaped formations deeper in the brick material. A typical image of the migration is illustrated in Fig. 5(a) and is found in both brick types. Fig. 5(b) shows needle-like formations with stoichiometric proportions $K_2O{\cdot}11Al_2O_3$ that are more profound in the bauxite based brick than in the andalusite based brick. The label used in the QEMSCAN analysis of this phase is corundum (K) and it is referred to in the literature as potassium-β-alumina [17]. Secondary mullite is formed around the mullite grains in the presence of alkali metals in both brick types, shown in Fig. 5(c). In the QEMSCAN images the secondary mullite is called mullite needles in alkali glass.

The tests show that the brick with higher corundum content (bauxite based) have a less distinct penetration front and the corundum grains stay more intact. The alkali metals have migrated along the grain boundaries in the high corundum brick, while the andalusite based brick create a reaction layer, shown in Fig. 5(d). Such reaction layer is reported to prevent further slag penetration [17] and consists of nepheline [18] that forms a dense layer through a volume expansion, outside the layer of secondary mullite. Also observed, is that the slag adheres harder to the andalusite based brick.

From the reaction test with 72 h dwell time at 1400 °C, the corundum and hematite solid solution have further increased in concentration (Fig. 6), and appears as needle-like formations in both bricks. The white regions adjacent to the needles are hematite with the presence of titanium and without aluminium. Thus the corundum/hematite solid solution is Ti depleted while it retains Al. Most of the alkali metals have evaporated or migrated out of the slag and into the brick. The progression of the reaction zone is therefore affected by the lack of alkali metals to drive the zone further. Noteworthy is that the protective nepheline reaction layer observed in the andalusite based brick after 72 h, is now lost and the penetration front looks similar in both crucible types.

3.2. Thermodynamic simulations

The composition of the system used for the first thermodynamic simulation was:

- 5 g of $3Al_2O_3{\cdot}2SiO_2$ (mullite).
- 1 g of K_2CO_3.
- 1 g of Na_2CO_3.

This is an approximation of the composition in the brick crucible tests when excluding hematite. The result of the simulation is shown in Fig. 7(a) as phase fraction as a function of temperature. The simulation is based on reaching equilibrium at

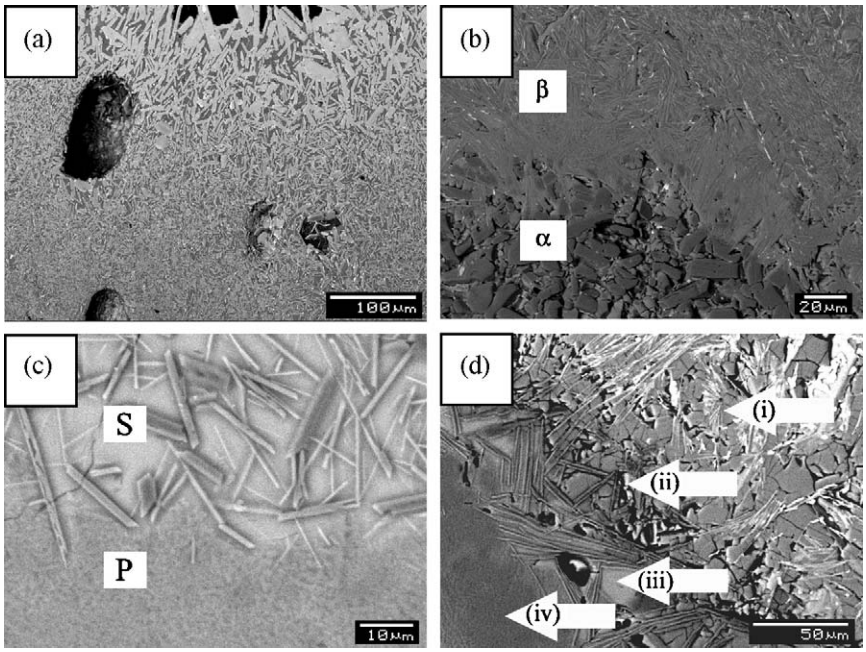

Fig. 5. Backscattered electron micrographs that shows: (a) hematite migrated through the dissolved brick in needle-shaped formations, (b) formation of potassium-beta-alumina, and (c) formation of secondary mullite; all from the Victor HWM crucible in the test at 1400 °C (5 h), and (d) the reaction layer between mullite and slag, from the Silox 60 crucible in the test at 1400 °C (5 h). Seen in image (d) is: (i) hematite in needle formations in the slag phase, (ii) formation of nepheline together with mullite needles, (iii) secondary mullite, and (iv) primary mullite.

every temperature, which results in reactions between alkali metals, mullite and corundum at considerably lower temperatures than what is experimentally observed. Only solid phases and gaseous (not shown) are considered. The Al_2O_3 and the mullite are already disintegrated at 550 °C when the simulation starts. Instead $K_2Al_{12}O_{19}$, $NaAlSiO_4$, $KAlSiO_4$, and Na_2CO_3 appear. At 700 °C the Na_2CO_3 disappear, and $KAlO_2$ forms. The largest variation in concentrations is at 1100 °C when $K_2Al_{12}O_{19}$ totally disappear to the benefit of KAl_9O_{14}.

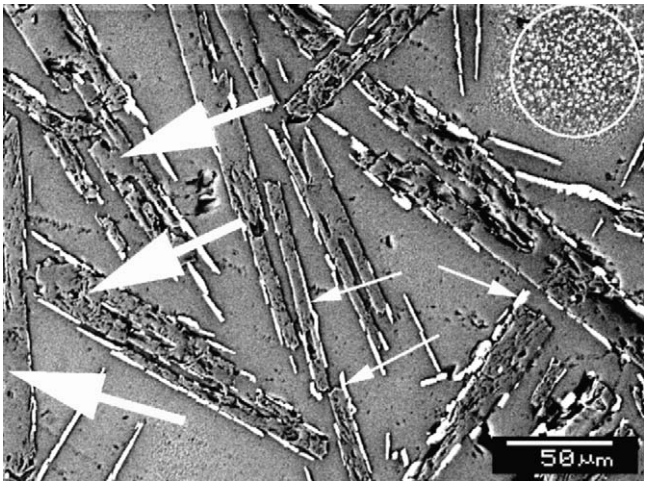

Fig. 6. Backscattered electron micrograph from the Silox 60 crucible test at 1400 °C (72 h). Large arrows to right mark the needle formations of the corundum–hematite solid solution, small arrows to right in the image mark the periphery of these needles that consists of hematite with Ti, depleted of Al, the circle marks hematite grains in snow flake formations, in an alumina–silicate matrix.

In a second thermodynamic simulation 5 g of Fe_2O_3 (hematite) was added to the previous starting composition. The result of the simulation is shown in Fig. 7(b).

The difference between the two simulations is that in the second case with Fe_2O_3 addition, Al_2O_3 and Fe_2O_3 forms a solid solution (labeled corundum) already at the starting temperature, which at most, incorporate ~10% Al_2O_3. At temperature above 1200 °C this phase transform to a spinel phase, which above 1250 °C also incorporate Al_2O_3 from the KAl_9O_{14}, which then increase its amount.

4. Discussion

This work focus on the degradation of bricks serving as refractory liners in rotary kilns at iron ore pellet production, i.e. characterization of occurring chemical reactions and alkali metal migration in mullite based refractories. The observed reactions between brick and slag are as expected more enhanced by increased temperature compared to increased dwell time, both in terms of penetration depth of slag into the bricks, corrosion of the bricks, and how the slag adheres to the brick surface. Micrographs reveal that alkali metals react primarily with mullite, and secondarily with Al_2O_3, forming β-Al_2O_3 which is expected based on the literature [17,19]. The penetration front is less distinct in the bauxite based brick, where corundum exists in higher amounts. Corundum grains keep more intact than mullite grains but the grain boundaries corrode and the grains migrate into the slag. The slag adheres harder to the andalusite based brick that has a lower corundum concentration.

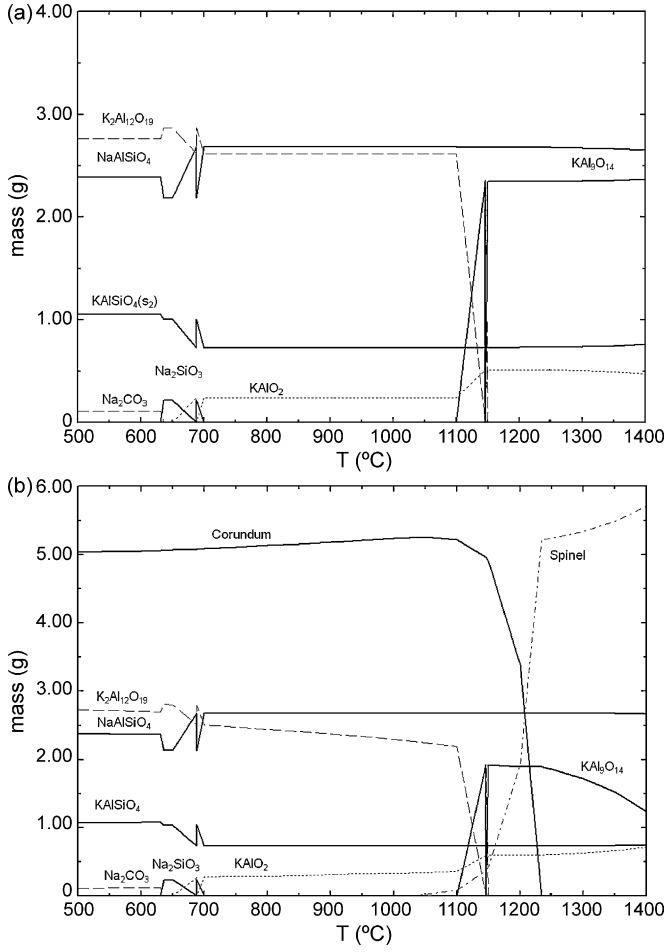

Fig. 7. Thermodynamic simulation of a system consisting of (a) mullite, K_2CO_3, and Na_2CO_3, and (b) mullite, hematite, K_2CO_3, and Na_2CO_3; both carried out between 500 and 1400 °C in argon atmosphere at ambient pressure.

The interaction between slag and bricks observed in this study can be described as: grains of hematite with sizes between 50 and 100 μm remain at the original surface of the brick. Hematite species, migrates and penetrates through the partly dissolved and porous brick by capillary infiltration and diffusion, and forms in needle-shaped crystals deeper in the lining material. Hematite has an isomorphic structure to corundum and to some extent forms a solid solution according to the thermodynamic simulations, which is also seen experimentally as these needle-like formations. Below the layer of dissolved brick that contains these two types of hematite needles, another layer of β-alumina and feldspathoids are formed, seen experimentally and in accordance with the thermodynamic simulations. This disintegration of mullite that results in the formation of nepheline is associated with a volume expansion, observed by dilatometry to occur fastest between 650 and 750 °C [18] and in some cases causing cracks in the tested crucibles. A third deeper layer with secondary mullite forms by the molten feldspar present during the heat treatment. Mullite in needle-like formations in an alkali metal rich glass is in accordance with earlier observations [20–23], where nucleation of primary mullite occurred in an amorphous silica glass (sizes less than 0.5 μm), and the alumina richer secondary mullite started to grow from the primary mullite, in needle-shaped formations (lengths above 1 μm) in the presence of an amorphous alkali–aluminosilicate melt. Potassium that causes this transformation is the element that migrates deepest into the brick. Scudeller et al. [8] suggested that K_2O reacts with SiO_2, forming a glassy matrix. With time kaliophilite ($K_2O\ Al_2O_3{\cdot}2SiO_2$), the cubic form of kalsilite, is formed; and with longer time and depending on the presence of free SiO_2, leucite ($K_2O\ Al_2O_3{\cdot}4SiO_2$) is formed. At a dwell time of 72 h a high concentration of a glassy alumina silicate matrix is present, especially in the andalusite based brick, which further enhances the degradation of the brick [18].

Potassium beta-alumina (β-Al_2O_3) was observed as a reaction product in needle-like formations, which is in agreement with thermodynamic simulations that predict the presence of KAl_9O_{14} with similar composition. β-Al_2O_3 containing sodium and/or potassium are observed in the literature in needle-like formations [24] and with different molar ratios [8,17,24–26]; where the β′ and β″ phases contain an increasing amount of alkali metals. The β-Al_2O_3 is no longer present after for 72 h, to the benefit of the corundum (Fe) solid solution and the alumina silicate matrix. In order to improve the lifetime of the refractories primarily the penetration of potassium needs to be suppressed.

The corundum–hematite solid solution depleted of Ti formed after long dwell time at high temperatures (see in Fig. 6), has previously been observed [27–29] and is predicted by thermodynamic simulations (not shown). According to the literature, the Hem(*ss*) can incorporate 8% Al_2O_3, and the Cor(*ss*) can incorporate Fe_2O_3 8% at 800 °C. At 1300 °C the concentrations are increased to 12 and 15 wt% respectively. Above 1318 °C the phase $AlFeO_3$ is formed [30]. The maximum TiO_2 concentration in Fe_2O_3 at 1200 °C is 12.3 mol%, while Fe_2O_3 maximum concentration at 1200 °C in TiO_2 is 0.8 mol% [28]. The maximum TiO_2 concentration in Al_2O_3 is ∼0.3 mol%, while Al_2O_3 is not soluble in TiO_2 [29]. Titanium is instead often included by the phase pseudobrookite ($Fe_2O_3\ TiO_2$) on the form M_3O_5, a solid solution that can include other cations (e.g. Al^{3+}, Mg^{2+}) [31,32], or have a higher iron concentration similar to our experiment. A pseudobrookite with aluminium is often referred to as β-Al_2TiO_5. Another phase observed in the system, with confirmed stoichiometry $Al_6Ti_2O_{13}$ and orthorhombic crystal structure were synthesized by Norberg et al. [33]. Among these solid solutions between phases, observed in the literature [27–32], what satisfies best with our observation (Fig. 6) is a hematite incorporating Al_2O_3 (large arrows in figure) and a hematite incorporating TiO_2 (small arrows in figure), both depleted of TiO_2 and Al_2O_3 respectively.

5. Conclusions

- The presence of alkali metals cause several types of chemical reactions that are detrimental to the lifetime of both types of brick investigated.
- Potassium is more detrimental than sodium since it penetrates deeper in to the brick.

- The alkali metals penetrate deeper in the high corundum bricks, forming β-alumina, nepheline and kalsilite accompanied with a volume expansion that causes brick degradation through cracking.
- The slag adheres harder to the brick with lower corundum concentration.
- A protective reaction layer is formed in the low corundum brick, which only stays intact at lower temperatures and short dwell times.
- Grains of hematite, with sizes between 50 and 100 μm, were observed to remain on the origin surface of the brick, while hematite species migrates through the partly dissolved and porous brick bulk by capillary infiltration and diffusion, and forms needle-shaped crystals deeper in the lining material.
- At high temperature corundum and hematite forms a solid solution, which is depleted of Ti.

Acknowledgments

The authors are grateful for the help with chemical analysis from LKAB, and to Dag Thulin for fruitful discussions. J.S. is grateful for the financial support from LKAB.

References

[1] A.M. Garbers-Craig, How cool are refractory materials? The Journal of the South African Institute of Mining and Metallurgy 108 (2008) 1–16.
[2] S. Forsmo, Influence of green pellet properties on pelletizing of magnetite iron ore, Doctoral Thesis, Luleå University of Technology, ISSN: 1402-1544.
[3] V. Niiniskorpi, Grate–kiln–cooler. Where to oxidize and why? in: 61st Iron Making Conference Proceedings, Iron and Steel Society, 2002, pp. 533–542.
[4] T. Uenaka, H. Isako, K. Tokutake, K. Aketa, Coal firing in pelletizing plant developed by Kobe steel, Ironmaking and Steel making 10 (5) (1983) 234–239.
[5] H. Schneider, J. Schreuer, B. Hildman, Structure and properties of mullite—a review, Journal of the European Ceramic Society 28 (2) (2008) 329–344.
[6] Y.-C. Ko, Wear of refractories in the iron and steel industry, SEASAI Quarterly 20 (2) (1991) 19–29.
[7] A. Yamaguchi, Consideration on improving corrosion-resistance of refractories, Taikabutsu Overseas 13 (4) (1993) 3–7.
[8] L. Scudeller, E. Longo, J. Varela, Potassium vapor attack in refractories of the alumina–silica system, Journal of the American Ceramic Society 73 (5) (1990) 1413–1416.
[9] L.-G. Liu, High pressure phase transformations of albite, jadeite and nepheline, Earth and Planetary Science Letters 37 (3) (1978) 438–444.
[10] D Pirrie, A. Butcher, M. Power, P. Gottlieb, G. Miller, Rapid quantitative mineral and phase analysis using automated scanning electron microscopy (QEMSCAN); potential applications in forensic geoscience, Geological Society 232 (2004) 123–136.
[11] R. Pascoe, M. Power, B. Simpson, QEMSCAN analysis as a tool for improved understanding of gravity separator performance, Minerals Engineering 20 (5) (2007) 487–495.
[12] A. Butcher, T. Helms, P. Gottlieb, R. Baterman, S. Ellis, N. Johnson, Advances in the quantification of gold deportment by QEMSCAN, in: Proceedings of the 7th Mill Operators Conference, 2000, pp. 267–271.
[13] P. Gottlieb, G. Wilkie, D. Sutherland, E. Ho-Tun, S. Suthers, K. Perera, B. Jenkins, S. Spencer, A. Butcher, J. Rayner, Using quantitative electron microscopy for process mineralogy applications, Journal of the Minerals, Metals and Materials Society 52 (4) (2000) 24–25.
[14] Y. Liu, R. Gupta, T. Wall, Ash formation from excluded minerals including consideration of mineral–mineral associations, Energy & Fuel 21 (2) (2007) 461–467.
[15] B. Benvie, Mineralogical imaging of kimberlites using SEM-based techniques, Minerals Engineering 20 (5) (2007) 435–443.
[16] W. Goodall, P. Scales, A. Butcher, The use of QEMSCAN and diagnostic leaching in the characterisation of visible gold in complex ores, Minerals Engineering 18 (8) (2005) 877–886.
[17] R. Farris, J. Allen, Aluminous refractories—alkali reactions, Iron and Steel Engineering 50 (2) (1973) 67–74.
[18] J. Stjernberg, M.-L. Antti, L.-O. Nordin, M. Odén, Degradation of refractory bricks used as thermal insulation in rotary kilns for iron ore pellets production, Applied Ceramics Technology 6 (6) (2009) 717–726.
[19] J.F. Schairer, N.L. Bowen, The system K_2O–Al_2O_3–SiO_2, American Journal of Science 253 (12) (1955) 681–746.
[20] Y. Iqbal, W. Lee, Fired porcelain microstructures revisited, Journal of the American Ceramic Society 82 (12) (1999) 3584–3590.
[21] Y. Iqbal, W. Lee, Microstructural evolution in triaxial porcelain, Journal of the American Ceramic Society 83 (12) (2000) 3121–3127.
[22] W. Lee, Y. Iqbal, Influence of mixing on mullite formation in porcelain, Journal of European Ceramic Society 21 (14) (2001) 2583–2586.
[23] M. Ribeiro, D. Tulyagavov, J. Ferreira, Labrincha, High temperature mullite dissolution in ceramic bodies derived from Al-rich sludge, Journal of European Ceramic Society 25 (5) (2005) 703–710.
[24] J. Tulliani, L. Dessemond, C. Esnouf, Role of a sodium glassy binder on microstructure and electrical conductivity of beta-alumina-based gas sensors, Ceramics International 30 (4) (2004) 525–532.
[25] E. Yazhenskikh, K. Hack, M. Müller, Critical thermodynamic evaluation of oxide system relevant to fuel ashes and slags. Part 2. Alkali oxide–alumina systems, CALPHAD 30 (4) (2006) 397–404.
[26] H. Näfe, K. Shqau, Determination of the potassium activity in the heterogeneous phase system K-beta-Al_2O_3/borate glass, MeO/Me, Journal of Chemical Thermodynamics 37 (1) (2005) 1–5.
[27] R. Venkataraman, R. Krishnamurthy, Evaluation of fracture toughness of as plasma sprayed alumina–13 wt.% titania coatings by micro-indentation techniques, Journal of the European Ceramic Society 26 (15) (2006) 3075–3081.
[28] M. Pownceby, M. Fisher-White, V. Swamy, Phase relations in the system Fe_2O_3–Cr_2O_3–TiO_2 between 1000 and 1300 °C and the stability of (Cr,Fe)2$Ti_{n-2}O_{2n-1}$ crystallographic shear structure compounds, Journal of Solid State Chemistry 161 (1) (2001) 45–56.
[29] M. Pownceby, K. Constanti-Carey, M. Fisher-White, Subsolidus phase relationships in the system Fe_2O_3–Al_2O_3–TiO_2 between 1000° and 1300 °C, Journal of the American Ceramic Society 86 (6) (2004) 975–980.
[30] A. Muan, C. Gee, Phase equilibrium studies in the system iron oxide–Al_2O_3 in air and at 1 atm. O_2 pressure, Journal of the American Ceramic Society 39 (6) (1956) 207–214.
[31] Y.H. Zhang, A. Reller, Nanocrystalline iron-doped mesoporous titania and its phase transition, Journal of Materials Chemistry 11 (10) (2001) 2537–2541.
[32] I. Grey, L. Cranswick, C. Li, T. White, L. Bursill, New M_3O_5-anatase intergrowth structures formed during low-temperature oxidation of anosovite, Journal of Solid State Chemistry 150 (1) (2000) 128–138.
[33] S. Norberg, S. Hoffman, M. Yoshimura, N. Ishizawa, $Al_6Ti_2O_{13}$ a new phase in the Al_2O_3–TiO_2 system, Acta Crystallographica Section C C61 (3) (2005) i35–i38.